RESEARCH ARTICLE

Mitochondrial dynamics and quantification of mitochondria-derived vesicles in cardiomyoblasts using structured illumination microscopy

Ida S. Opstad[1*] | Gustav Godtliebsen[2] | Balpreet Singh Ahluwalia[1,3] |
Truls Myrmel[2,4] | Krishna Agarwal[1] | Åsa Birna Birgisdottir[2,4]

[1]Department of Physics and Technology, UiT – The Arctic University of Norway, Tromsø, Norway

[2]Department of Clinical Medicine, UiT – The Arctic University of Norway, Tromsø, Norway

[3]Department of Clinical Science, Intervention and Technology, Karolinska Institute, Stockholm, Sweden

[4]Division of Cardiothoracic and Respiratory Medicine, University Hospital of North Norway, Tromsø, Norway

*Correspondence
Ida S. Opstad, Department of Physics and Technology, UiT – The Arctic University of Norway, Tromsø, Norway.
Email: ida.s.opstad@uit.no

Present address
Ida S. Opstad, Balpreet Singh Ahluwalia and Krishna Agarwal, Institutt for fysikk og teknologi, UiT Norges Arktiske Universitet, Teknologibygget, Tromsø, Norway

Abstract

Mitochondria are essential energy-providing organelles of particular importance in energy-demanding tissue such as the heart. The production of mitochondria-derived vesicles (MDVs) is a cellular mechanism by which cells ensure a healthy pool of mitochondria. These vesicles are small and fast-moving objects not easily captured by imaging. In this work, we have tested the ability of the optical super-resolution technique 3DSIM to capture high-resolution images of MDVs. We optimized the imaging conditions both for high-speed video microscopy and fixed-cell imaging and analysis. From the 3DSIM videos, we observed an abundance of MDVs and many dynamic mitochondrial tubules. The density of MDVs in cells was compared for cells under normal growth conditions and cells during metabolic perturbation. Our results indicate a higher abundance of MDVs in H9c2 cells during glucose deprivation compared with cells under normal growth conditions. Furthermore, the results reveal a large untapped potential of 3DSIM in MDV research.
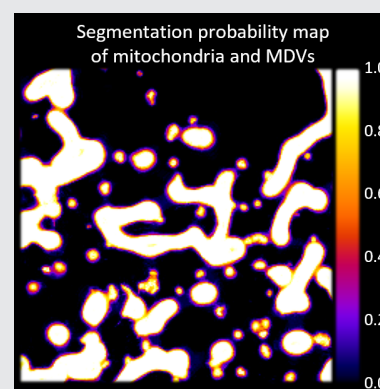
KEYWORDS

3DSIM, cardiomyoblasts, MDVs, mitochondria, mitochondria tubules, mitochondria-derived vesicles, three-dimensional structured illumination microscopy, Trainable Weka Segmentation

Segmentation probability map of mitochondria and MDVs

1 | INTRODUCTION

Mitochondria are the energy providing organelles in cells and produce energy in the form of adenosine triphosphate (ATP). Mitochondria are comprised of four major compartments: the outer mitochondrial membrane, the inter-membrane space, the inner mitochondrial membrane with invaginations termed cristae and

the matrix. In most cell types, mitochondria are arranged in highly dynamic networks controlled by frequent mitochondrial fusion and fission (division) events driven by mitochondria movements on the cytoskeleton [1]. Damaged mitochondria result in energy-generation defects, increased production of harmful reactive oxygen species (ROS) and show a greater tendency to trigger programmed cell death [2]. Hence, in order to ensure a healthy pool of mitochondria, cells employ different mitochondria quality control mechanisms [3] to maintain normal cell function.

Mitochondria-derived vesicles (MDVs) act in mitochondria quality control. These are small (70–150 nm in diameter), single or double-membrane vesicles that arise through budding from the mitochondria and are induced under stress conditions [4]. MDV populations have previously been defined and classified as translocase of the outer mitochondria membrane 20 (TOMM 20, outer membrane) positive or pyruvate dehydrogenase (PDH, matrix protein) positive [4]. However, several other mitochondria resident proteins (matrix or inner membrane-associated) have been identified on MDVs [5–7] indicating their heterogeneous nature.

The MDVs' size and dynamic nature pose a challenge for conducting imaging studies (particularly for live imaging) of their formation and trafficking. Elucidation of their significance for mitochondria homeostasis as well as cell function in general is important, especially in high-energy demanding cardiac cells.

Previously, the formation and dynamics of TOMM 20 positive MDVs in Vero cells were observed at a rate of 10 frames per second using an ultrafast spinning disk super-resolution microscope developed as a high-speed alternative to SIM [8]. However, the high speed comes at a cost of compromised optical sectioning ability and poorer signal-to-noise ratio (SNR). Furthermore, no quantification of the vesicles was conducted in this work.

The acquisition of images at high enough resolution and contrast to allow MDVs to be visualizable by eye is a significant challenge, but not the only hurdle in gathering knowledge about MDVs. Other significant challenges are the appropriate labeling for super-resolution microscopy (e.g., bright, photostable and specific fluorescent markers) and the quantification of these small and (in living cells) dynamic structures. Using traditional hard thresholding methods for MDV quantification is challenging because of the vesicles' low signal compared with the noise level and the presence of image reconstruction artifacts.

In this work, we investigated the capabilities of three-dimensional structured illumination microscopy (3DSIM) for visualizing and quantifying MDVs in live and fixed H9c2 cardiomyoblasts with a stable expression of a fluorescent transmembrane domain of the outer mitochondria membrane protein 25 (OMP25) [9]. The technique requires the acquisition of 120 modulated images per 1 μm image volume per color channel and, hence, is not as fast as spinning disk microscopy, but benefits from three-dimensional resolution doubling compared with conventional microscopy. Using 3DSIM, we optimized the acquisition conditions for high-speed and up to 100 time-points super-resolution volumetric imaging. To quantify and compare the number of fluorescently-tagged OMP25 MDVs produced under normal (GLU) and glucose-deprived (galactose adapted, GAL) growth conditions, we applied Trainable Weka Segmentation (TWS). Replacing glucose in the growth media with galactose forces cells in culture to become more oxidative and has been shown to facilitate stress-induced MDV production [10, 11].

2 | METHODS

2.1 | Cell-culture and sample preparation

The rat cardiomyoblast cell-line H9c2 (cells derived from embryonic heart tissue; Sigma Aldrich) was genetically modified using a retrovirus to achieve a stable expression of tandem tagged (mCherry-EGFP) mitochondrial outer membrane protein 25 (OMP25)-transmembrane domain (TM). A uniform expression of fluorescence intensity in the cells was achieved through flow cytometry sorting. The stable H9c2 cells were cultured in high glucose (4.5 g/L) Dulbecco's Modified Eagle Medium (DMEM; [D5796, Sigma-Aldrich]) with 10% FBS, 1% streptomycin/penicillin and 1 μg/mL of puromycin (InvivoGen). For glucose deprivation and adaptation to galactose, the cells were grown in DMEM without glucose (11966-025, Gibco) supplemented with 2 mM L-glutamine, 1 mM sodium pyruvate, 10 mM galactose, 10% FBS, 1% streptomycin/penicillin and 1 μg/mL of puromycin (InvivoGen). The cells were adapted to galactose for a minimum of 7 days before experiments. The cells were seeded on MatTek dishes (P35G-1.5-14-C, MatTek Corporation) and imaged when they reached approximately 80% confluency.

2.1.1 | Cell fixation

The cells were fixed using either 4% paraformaldehyde (PFA) or 4% PFA + 0.2% glutaraldehyde (GA) in phosphate-buffered saline (PBS, preheated to 37°C) for 30 minutes at room temperature. The samples were then washed and re-immersed in PBS before imaging.

2.1.2 | Imaging conditions

The living cells were imaged in their usual growth media at 37°C with atmospheric gas levels. The fixed samples were imaged at either room temperature or 37°C.

2.2 | Microscope

The images were acquired using a DeltaVision OMX V4 Blaze imaging system (GE Healthcare) equipped with a ×60 1.42 NA oil-immersion objective (Olympus), three sCMOS cameras and 405, 488, 568 and 642 nm lasers for excitation. The vendor-specified optical resolution of the 3DSIM system is 110–160 nm laterally and 340–380 nm axially, depending on color channel. To surpass the diffraction limit, this SIM set-up uses sinusoidal illumination patterns and acquires 120 images per 1 μm z-stack thickness (three illumination angles times five phase shifts times 8 planes/μm thickness) per color channel. Super-resolution 3DSIM images are then obtained via image processing using the manufacturer-supplied Soft-WoRx program.

2.2.1 | Optimization of imaging speed and differences between fixed cell and live-cell image data

To maximize the system imaging speed for as accurate as possible detection of fast-moving MDVs in living cells, the following differences were implemented compared with for fixed cell imaging:

The camera mode was changed from "Medium" low-noise sCMOS readout rate (95 MHz, rolling shutter) to "Fast" readout (286 MHz, global shutter), increasing the camera read noise by about 33% (from 1.5 e to 2 e), while reducing possible motion-induced image artifacts (presuming a larger effect for fast-moving objects).

The camera read area was reduced to 1/4 from the normal for SIM field-of-view (FOV, used for the fixed samples) of 512 × 512 pixels (41 × 41 μm^2) to 256 × 256 pixels (20.5 × 20.5 μm^2)

The selection of image volume was done sparingly with careful selection of the lower and upper cell boundaries. For the live imaging (with smaller FOVs), volumes avoiding the thicker cell area close to the nucleus allowed for a higher volumetric frame rate without losing significant parts of the mitochondria and MDVs moving axially during video acquisition. This reduced the stack size (and acquisition time) up to three times, from about 3 μm to 1–2 μm. Stack sizes down to 1.0 μm were acquired, but

here in some cases, mitochondria appear to move out of the acquired volume axially, indicating a too sparingly chosen image volume. For the larger images used for the fixed-cells, the cell nuclear region was included, resulting in stack sizes of instead 3–3.5 μm to cover the entire cell volume of the captured area.

The camera exposure time was changed by a factor of four, from 20 ms (fixed samples) to 5 ms for the live samples (both with 10% transmission of 0.10 W lasers, not including the loss in the optical path of at least 50%). This was the shortest exposure time that could be used without too severely compromising the SIM reconstruction quality or at a significantly increased rate of photobleaching (especially relevant for time-lapse studies).

Under these conditions (employed for the data of Figure 1), the live acquisition of a 2.0 μm thick volume (single channel) took 1.50 s. Volumes of 1.0 μm thickness took down to 1.16 s. In comparison, the fixed cell 3DSIM images (512 × 512 pixels and 3.0 μm thickness) had an acquisition time of 12.0 s. Taken together, *the 3DSIM image acquisition time was reduced up to 10 times* compared with the fixed cell (and normally employed) acquisition parameters.

2.3 | Image processing

2.3.1 | Image reconstruction and channel registration

Image deconvolution and 3DSIM reconstructions were completed using the manufacturer-supplied SoftWoRx program (GE Healthcare). Image registration (color channel alignment) was also performed in the same program using experimentally measured calibration values compensating for minor lateral and axial shifts, rotation and magnification differences between cameras. The pixel area of the 3DSIM images is 1/4 of the acquired raw data (40 nm × 40 nm after SIM reconstruction vs. 80 nm × 80 nm for raw data). The processed 3D images were then maximum intensity z-projected as a final step.

2.3.2 | Image analysis and processing

Image analysis and processing beyond the preprocessing described above was done using Fiji/ImageJ [12]. The mitochondria vesicle segmentation and quantification were done with help of TWS, a machine learning tool for pixel classification in microscopy images [13].

The TWS training was conducted for two manually annotated classes (background and mitochondria) using
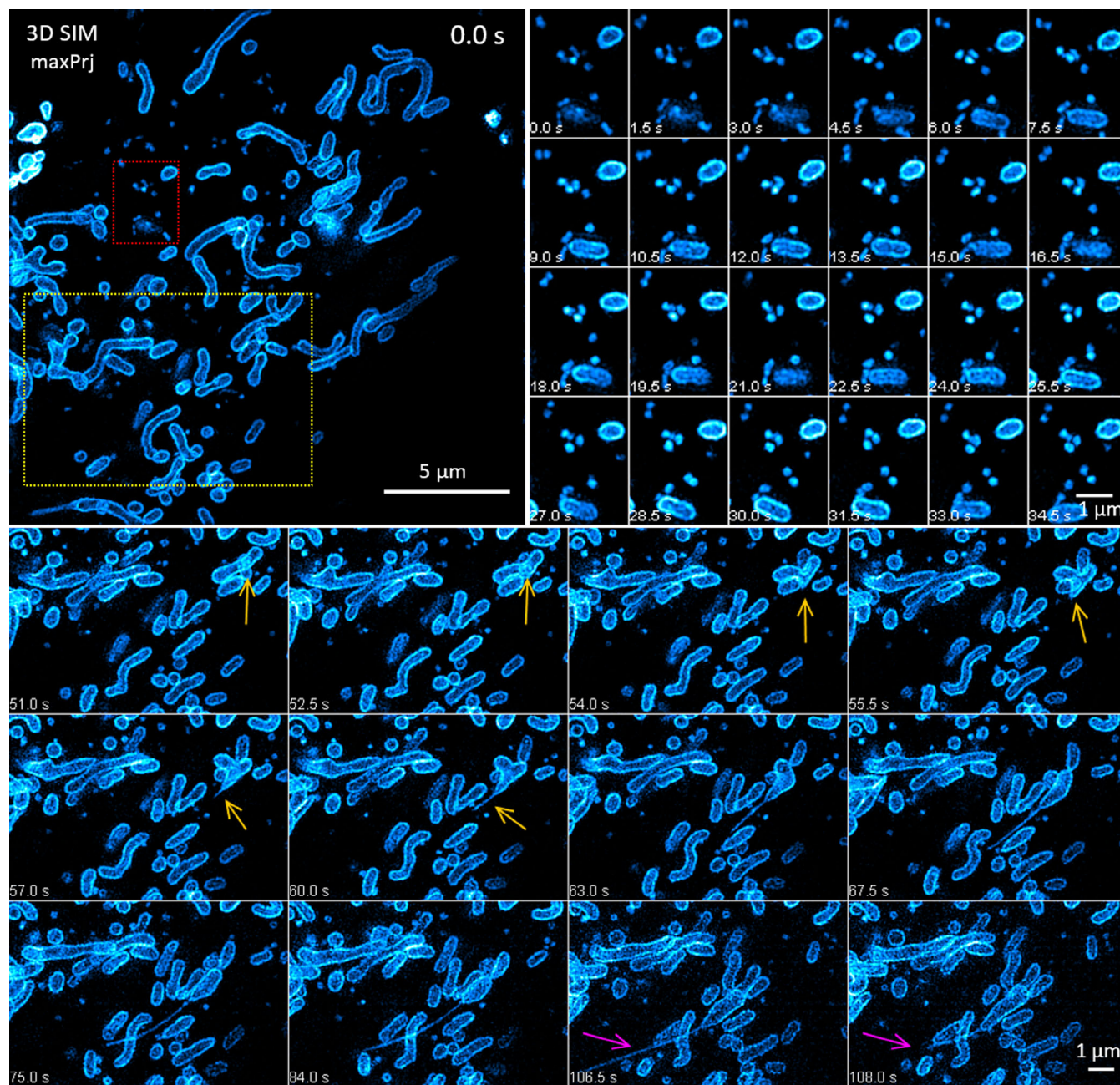
FIGURE 1 Fast 3DSIM time-lapse of MDVs and dynamic mitochondrial tubules in H9c2 cells (outer mitochondrial membrane, EGFP) cultivated in galactose medium. A part of the vesicle dynamics denoted by the small red box is shown on the left. Here, the vesicles in the upper left part of the panels are seen to interact dynamically with each other, while the vesicles and nanorods toward the bottom of the frames are interacting with a much larger mitochondrion (0–25.5 s). In the bottom row panels, the MDVs appear to both fuse and bud-off from the lower mitochondrion (27–34.5 s). The yellow box is shown in the bottom montage for selected subsequent time-points. The yellow arrows show the formation of a tubule, while the magenta arrows indicate the rapid retraction (several micrometers in 1.5 s) of the same tubule about 10 s later. The shown time-sequence has been intensity corrected for photobleaching (exponential fit). The full time-lapse is available as Movie S1

FastRandomForest and all other default options. The supervised training of the classifier was done using one maximum intensity projected 3DSIM image of fixed (4% PFA + 0.2% GA) cells from the GAL conditions with both clearly visible MDVs and SIM reconstruction artifacts (the annotation was done by a SIM expert). SIM artifacts were added to the background class of the training set to avoid these intensity patterns to be classified as mitochondria (or MDVs). The classifier was then applied to both the live and fixed samples from both pools (GAL

and GLU). Probability maps were generated and the segmentation threshold was chosen at 0.80 after manual inspection and comparison with the raw data of both live and fixed samples.

A couple of outliers where the learned classifier did not achieve satisfactory results were removed from the dataset before quantification. These are shown and discussed in Figure S1.

3 | RESULTS AND DISCUSSION

3.1 | 3DSIM of MDVs and dynamic mitochondrial tubules

The optimized acquisition conditions for high-speed and lowest possible laser illumination intensity—while still achieving good 3DSIM reconstruction—enabled capturing videos of the delicate and fast-moving OMP25-TM positive MDVs in H9c2 cells at volumetric super-resolution for up to 100 time-points. A part of such a time-lapse is shown in Figure 1, with the large top panel showing an overview of the volumetric super-resolution image. The full time-lapse (maximum intensity z-projected 3DSIM images) is provided in Movie S1. The highest volumetric imaging speed achieved was 1.5 s for image volumes of $20.5 \times 20.5 \times 2.0 \ \mu m^3$. Higher imaging speeds could be achieved for even smaller volumes, but then greatly reducing the likelihood of capturing interesting biological events in a subcellular context.

In addition to an abundance of MDVs, several rapidly extending and retracting tubules derived from the mitochondrial outer membrane were observed in cells cultivated under both GLU and GAL conditions. An example of a rapidly extending and retracting tubule over a time span of about a minute is shown and indicated by arrows in the lower part of Figure 1. At its longest, this tubule extended to about 5 μm away from the mitochondrion from which it formed, and with a width of about 120 nm (FWHM of the tubule in the maxPrj 3DSIM image), corresponding to the lateral SIM resolution (GFP channel). The actual width of the tubule could be much narrower, but that is not measurable using this imaging technique. For the retracting tubule pointed out by the arrow in magenta color (106.5–108 s), the retraction appears to be occurring at a speed of several micrometers per second.

Such dynamic mitochondrial tubulation has previously been detected by SIM imaging in normal rat kidney cells (NRK) as well as in several other cell lines [14]. Recently, dynamic mitochondrial tubules were studied in COS-7 cell-line where they were shown to mediate transportation of mitochondrial DNA between different mitochondria [15]. However, mitochondrial tubulation has

previously not been demonstrated in H9c2 cardiomyoblasts. Interestingly, mitochondrial tubules have similarities to nanotunnels formed between mitochondria in cardiomyocytes [16]. In Movies S2 and (magnified view) S3, some of the tubules fuse with other mitochondria to form a temporary membrane bridge between two different mitochondria. A tubule can then subsequently detach from the originating mitochondria and remain attached to the recipient mitochondria. Interestingly, also the budding of a fragment was detected from a retracting tubule. A magnified view of this phenomenon is provided in Movie S4. Our measurements of the speed of these tubules are within the range of velocities measured for the tubules in COS-7 cells [17].

Next, we present a simple but effective semi-automatic analysis pipeline to quantify and compare the number of MDVs in cultured H9c2 cells under different conditions.

3.2 | Quantification of vesicles in live and fixed cells

Two different strategies were employed to quantify and compare the number of MDVs between H9c2 cells cultivated under either GLU or GAL conditions: Either live-cell imaging using small imaging volumes ($840.5 \ \mu m^3$) or fixed-cell conditions using six times larger volumes ($5043 \ \mu m^3$). The two different strategies entail different advantages and limitations. For the live-cell imaging strategy, we ensure that no vesicles are lost or destroyed during fixation. On the other hand, due to the unwanted effect of motion artifacts in the SIM images, only small volumes were acquired, reducing throughput for statistical inferences. For the fixed-cell case, we risk no motion-related artifacts such that larger volumes and better statistics (per imaging time) can be inferred. Also, the nature of fixed samples allows for an easier comparison of different conditions without risking effects from possible time delays between and during imaging experiments. On the downside, the process of fixation can alter the biology we wish to study, and it can be hard to assess how this compares to the live-cell condition.

Two different protocols for chemical preservation of the cells were tested: either fixation using 4% PFA in PBS or 4% PFA + 0.2% GA in PBS. The results are shown in Figure 2, where a comparison with mitochondria in living cells is used as reference (Figure 1A). As shown in Figure 2B, using PFA only for fixation led to unsatisfactory preservation of the mitochondrial morphology at SIM resolution. Trying to segment MDVs from these images led to a high portion of false positives, where fragmented mitochondria—seemingly part of a continuous
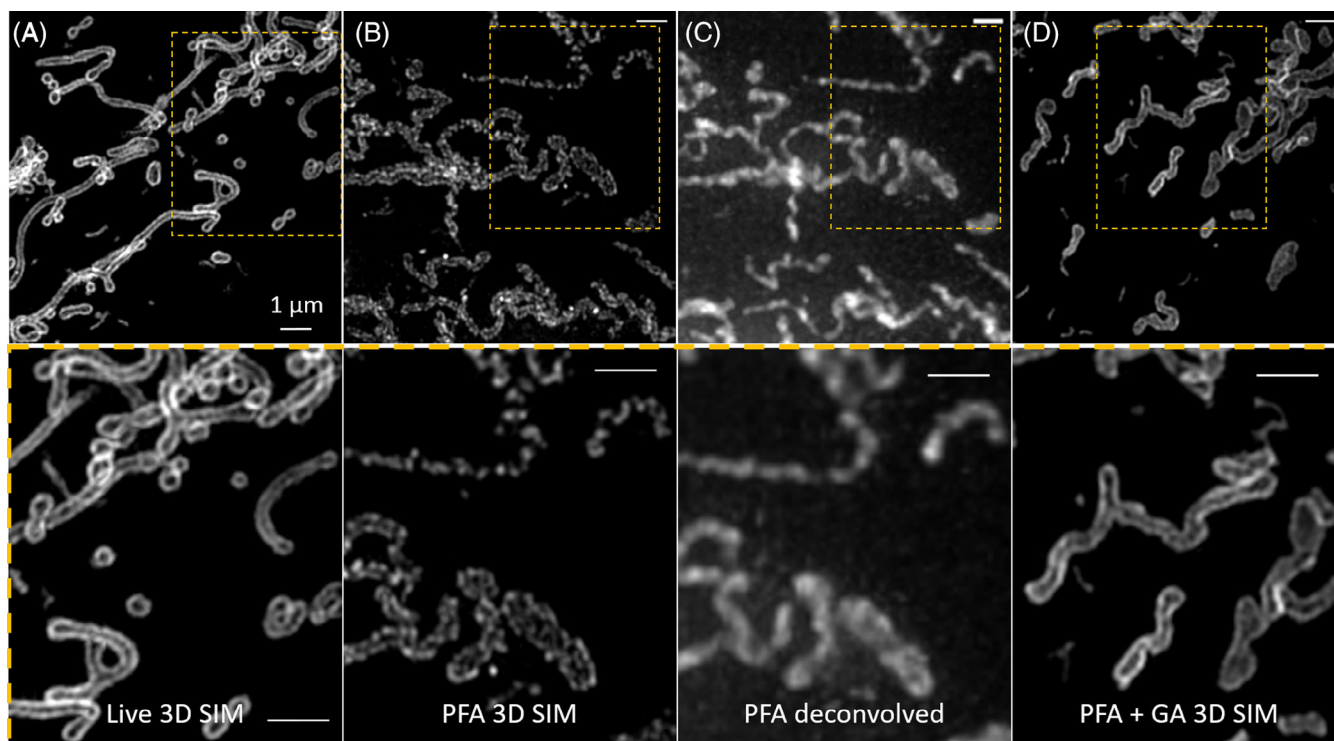
FIGURE 2 Comparison of live and fixed mitochondrial morphologies. The regions indicated in the upper panels A–D are displayed magnified below. Fixation using paraformaldehyde (PFA) only (panels B and C) causes fragmentation and disruption of the mitochondrial network as observed for living samples (panel A) hindering reliable MDV quantification. This effect is difficult to notice at conventional resolution (deconvolved image, panel C). Applying a fixation solution additionally containing glutaraldehyde (GA) preserves the live mitochondrial morphology much better and can be used for quantifying MDVs in fixed samples (panel D). The images are maxPrj 3DSIM images of H9c2 cells from the normal cultivation condition (GLU). Scale bars: 1 μm

structure before chemical fixation—would be counted as many additional MDVs not actually present. At conventional optical resolution (like the deconvolved image example in Figure 2C), this effect is much harder to notice and may be unimportant for some types of quantification of mitochondria. However, the analysis of MDVs—which are smaller than the resolution limit—requires the use of super-resolution techniques like 3DSIM for accurate quantification, together with a more potent fixation method than PFA alone. Preservation using both PFA and GA (Figure 2D) gave satisfactory results, resembling the live-cell imaging results even at SIM resolution (compare panels A and D of Figure 2) and showing MDVs unlikely to appear from fixation-induced mitochondrial fragmentation. A different challenge concerning GA fixed samples is the added background signal from GA autofluorescence. We noted additional artifacts in the SIM images likely resulting from this origin.

To overcome the challenges of MDV quantification in the presence of both SIM reconstruction artifacts (often of similar size and intensity level as the MDVs) and comparatively large and bright mitochondria, we employed TWS for MDV segmentation prior to quantification.

The pixelwise TWS classifier was trained using supervised learning on two classes: Background and Mitochondria. The annotated regions used for training the classifier together with the rest of the particle quantification workflow are shown in Figure 3.

To reduce the impact of SIM artifacts, lower axial resolution and to facilitate the assessment of classifier performance, only maxPrj 3DSIM images were used both for training and MDV quantification. The main loss of information from this simplification is that the MDVs located directly above or below the mitochondria are not counted. Since the images are 10–20 times larger laterally than axially, and the volume thickness only constitute about five resolution units laterally (for 2 μm stacks) versus 170 resolution units in either lateral dimension (for 20.2 μm images), we considered this a valid simplification only improving the accuracy of the particular analysis.

The training conducted on a fixed GLU cell (with visible SIM artifacts relegated to the background class) showed good transfer learning to both GAL and live-cell images (of smaller size). The manually assessed segmentation results were found satisfactory for all except two cases (discarded from the MDV quantification) of the
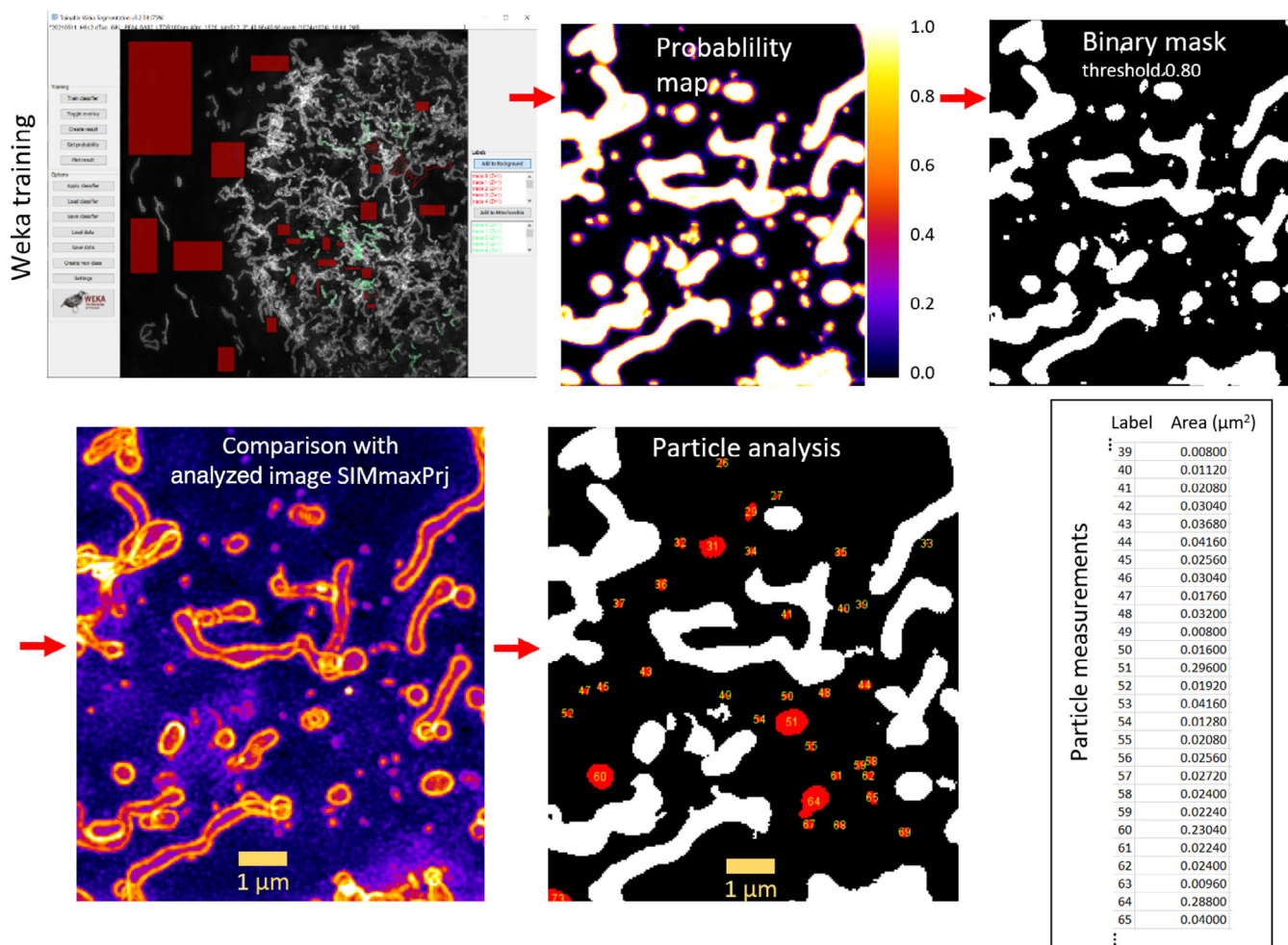
FIGURE 3 Segmentation of mitochondria for MDV quantification was done in ImageJ/Fiji using TWS. First, a maximum intensity z-projected (maxPrj) 3DSIM image was annotated with regions from the two classes *background* (including SIM artifacts) and *mitochondria*. Then the classifier was trained and applied to the remaining data of both live and fixed cells from both the GAL and GLU growth conditions. A probability map was chosen as output and a threshold of 0.80 was chosen as a binary mask for the mitochondria class. This was chosen after visual inspection and comparison with the SIM images to yield a satisfactory segmentation. The MDVs were measured from the binary images using Analyze Particles in ImageJ, excluding particles with a circularity <0.7 or not falling within the area range 0.0032 to 0.30 μm^2

TABLE 1 The number of MDVs measured per image, area and volume for GLU and GAL samples under both fixed and live imaging conditions

Sample condition	GLU		GAL	
	Live	Fixed	Live	Fixed
MDV/image	60 ± 26	127 ± 48	70 ± 31	223 ± 59
MDV/μm^2	0.14	0.076	0.17	0.13
MDV/μm^3	0.071	0.025	0.083	0.044

fixed-cell images that appeared particularly challenging due to two reasons:

1. Two different cells with distinct mitochondria morphology and brightness in the same image.
2. Dominating SIM reconstruction artifacts obscuring the actual cellular details.

Both of these fail cases are displayed in Figure S1.

The MDV quantification results are summarized in Table 1. Both the live- and fixed-cell imaging strategies yielded a higher vesicle number for cells under the GAL condition than under the GLU condition.

Quantification of MDVs in H9c2 cells has previously been conducted using confocal images of fixed cells with

immunofluorescent staining of TOMM20 and PDH mitochondria markers after galactose adaptation [11] or during normal (glucose) growth conditions [18]. The numbers of MDVs per cell obtained in these studies (10–30 MDVs per cell) are significantly lower than the numbers obtained here (the numbers per image cover less than one cell). Furthermore, a comparison of the number of MDVs in H9c2 cells under these different growth conditions was not investigated earlier.

The high standard deviations in Table 1 indicate that the particular state of individual cells also has a large impact on the number of MDVs, beyond growth conditions. Although the fixed images are of six times larger volumes (four times larger area), the number of MDVs was only 2.1 and 3.2 times higher (for GAL and GLU, respectively). The reason for this is can be a combination of several factors:

1. The inclusion of sparser parts of the samples with few or no MDVs, that is, especially the nuclear region and volumes completely outside of the cells.
2. The effect of z-projection is larger in the case of fixed samples as larger z-stacks were used for these. In effect, a larger portion of the vesicles could be invisible straight above or below brighter mitochondria.
3. Vesicles could be lost or destroyed during fixation and the subsequent sample washing steps.

Especially when considering volumetric cell densities of MDVs, the smaller image volumes (with carefully chosen volumetric boundaries) are likely to provide a more accurate estimate of the actual vesicle density inside cells, as the non-cell containing sample parts can be more accurately excluded. The cell boundaries could alternatively be determined with help of a membrane marker. However, due to the added cellular stress, experimental and analytical complexity associated with this membrane labeling, we instead used the distribution of mitochondria as a rough guide for cell boundaries.

4 | CONCLUSIONS

We have in this work explored the capability of 3DSIM for the challenging study of MDVs in living and fixed H9c2 cardiomyoblasts with a stable expression of a fluorescent mitochondria marker. The optimized high-speed imaging conditions enabled following mitochondria and MDVs at volumetric super-resolution for up to 80 time-points, each $20.5 \times 20.5 \times 2 \ \mu m^3$ volume with about 1.5 s acquisition time. In addition to a large number of MDVs, a multitude of rapidly extending and retracting mitochondrial tubules were observed for cells cultivated under both normal and galactose-adapted conditions. Interestingly, these nanotubules could be involved in the formation of MDVs.

Two different cell fixation approaches of the mitochondria for the purpose of MDV quantification were tested: 4% PFA and 4% PFA + 0.2% GA. Only the latter one was found suitable for the quantification of MDVs, as the PFA-only fixation led to the fragmentation of mitochondria and a misleadingly high number of MDVs.

Segmentation using the TWS machine learning tool provided satisfactory segmentation of mitochondria for the quantification of MDVs when the images contained mitochondria of single cells—and not of mitochondria of vastly different morphology and brightness as often the case in different adjacent cells—and for moderate SIM reconstruction artifacts. The SIM artifacts were largely successfully trained to be classified as part of the background class.

MDVs were quantified from TWS segmented images for both live and fixed conditions and their abundance was compared in normal and galactose-adapted cultivation conditions. Although varying largely within each group, the number of MDVs was on average found to be larger for the galactose-adapted condition than for the normal glucose-containing growth condition. This has previously not been demonstrated for H9c2 cells. Notably, COS-7 cell-line adapted to galactose did not display an increase in the number of MDVs compared with cells in glucose when exploiting confocal images of fixed and immunolabeled cells for MDV quantification [10]. The use of H9c2 cells with stable expression of a fluorescent mitochondria outer membrane marker and the application of super-resolution imaging display the advantage of our approach for both more accurate MDV detection and quantification.

Future work will involve MDV quantification of larger SIM image datasets from different growth conditions. In addition, analyzing the dynamics of MDVs will enable us to better assess their origin, fate, overall cellular function and, ultimately, their importance for the cardiovascular system [19].

CONFLICT OF INTEREST
The authors declare no conflicts of interest.

AUTHOR CONTRIBUTIONS

Åsa Birna Birgisdottir: Conceived the idea, provided expertise on cardiac cell biology, prepared a manuscript draft and conducted extensive review of relevant literature. **Ida S. Opstad:** Conducted the imaging experiments, data analysis, prepared a manuscript draft, image data archiving and prepared the figures and videos. **Gustav Godtliebsen:** Constructed the stable double-tag cell-line, cultivated the cells and advised on H9c2 sample preparation for microscopy. **Truls Myrmel:** Provided funding which enabled the project and experiments. **Krishna Agarwal:** Provided funding which enabled the project and experiments. **Balpreet Singh Ahluwalia:** Provided funding which enabled the project and experiments. All authors reviewed and commented on the manuscript.

DATA AVAILABILITY STATEMENT

The data that support the findings of this study are available from the UiT Open Research Data repository [19]. All image data (not only for the images shown) from these sets of experiments are provided as a community resource for, e.g., the further development of 3DSIM reconstruction algorithms, machine learning tools for bio-image analysis, and mitochondria research.

ORCID

Ida S. Opstad https://orcid.org/0000-0003-4462-4600
Balpreet Singh Ahluwalia https://orcid.org/0000-0001-7841-6952
Krishna Agarwal https://orcid.org/0000-0001-6968-578X
Åsa Birna Birgisdottir https://orcid.org/0000-0003-1080-3619

REFERENCES

[1] H.-M. Ni, J. A. Williams, W.-X. Ding, *Redox Biol.* **2015**, *4*, 6.

[2] D. A. Brown, J. B. Perry, M. E. Allen, H. N. Sabbah, B. L. Stauffer, S. R. Shaikh, J. G. F. Cleland, W. S. Colucci, J. Butler, A. A. Voors, S. D. Anker, B. Pitt, B. Pieske, G. Filippatos, S. J. Greene, M. Gheorghiade, *Nat. Rev. Cardiol.* **2017**, *14*(4), 238.

[3] S. Pickles, P. Vigié, R. J. Youle, *Curr. Biol.* **2018**, *28*(4), R170.

[4] A. Sugiura, G.-L. McLelland, E. A. Fon, H. M. McBride, *EMBO J.* **2014**, *33*(19), 2142.

[5] D. Matheoud, A. Sugiura, A. Bellemare-Pelletier, A. Laplante, C. Rondeau, M. Chemali, A. Fazel, J. J. Bergeron, L.-E. Trudeau, Y. Burelle, E. Gagnon, M. B. HM, M. Desjardins, *Cell* **2016**, *166*(2), 314.

[6] B. H. Abuaita, T. L. Schultz, M. X. O'Riordan, *Cell Host Microbe* **2018**, *24*(5), 625.

[7] K. Todkar, L. Chikhi, V. Desjardins, F. El-Mortada, G. Pépin, M. Germain, *Nat. Commun.* **2021**, *12*(1), 1.

[8] S. Hayashi, Y. Okada, *Mol. Biol. Cell* **2015**, *26*(9), 1743.

[9] Y. Wang, M. Serricchio, M. Jauregui, R. Shanbhag, T. Stoltz, C. T. di Paolo, P. K. Kim, G. A. McQuibban, *Autophagy* **2015**, *11*(4), 595.

[10] V. Soubannier, G.-L. McLelland, R. Zunino, E. Braschi, P. Rippstein, E. A. Fon, H. M. McBride, *Curr. Biol.* **2012**, *22*(2), 135.

[11] V. J. J. Cadete, S. Deschênes, A. Cuillerier, F. Brisebois, A. Sugiura, A. Vincent, D. Turnbull, M. Picard, H. M. McBride, Y. Burelle, *J. Physiol.* **2016**, *594*(18), 5343.

[12] J. Schindelin, I. Arganda-Carreras, E. Frise, V. Kaynig, M. Longair, T. Pietzsch, S. Preibisch, C. Rueden, S. Saalfeld, B. Schmid, J. Y. Tinevez, D. J. White, V. Hartenstein, K. Eliceiri, P. Tomancak, A. Cardona, *Nat. Methods* **2012**, *9*(7), 676.

[13] I. Arganda-Carreras, V. Kaynig, C. Rueden, K. W. Eliceiri, J. Schindelin, A. Cardona, H. S. Seung, *Bioinformatics* **2017**, *33*(15), 2424.

[14] C. Wang, D. Wanqing, Q. P. Su, M. Zhu, P. Feng, Y. Li, Y. Zhou, N. Mi, Y. Zhu, D. Jiang, S. Zhang, Z. Zhang, Y. Sun, L. Yu, *Cell Res.* **2015**, *25*(10), 1108.

[15] J. Qin, Y. Guo, B. Xue, P. Shi, C. Yang, Q. P. Su, H. Hao, S. Zhao, C. Wu, L. Yu, D. Li, Y. Sun, *Nat. Commun.* **2020**, *11*(1), 1.

[16] X. Huang, L. Sun, S. Ji, T. Zhao, W. Zhang, J. Xu, J. Zhang, Y. Wang, X. Wang, C. Franzini-Armstrong, M. Zheng, H. Cheng, *Proc. Natl. Acad. Sci. U. S. A.* **2013**, *110*(8), 2846.

[17] T. Zhao, H. Hao, Z. Wang, Y. Liang, K. Feng, M. He, Y. Xue, P. R. Bianco, Y. Sun, B. Yao, M. Lei, *Biomed. Opt. Express* **2021**, *12*(6), 3474.

[18] B. Li, H. Zhao, Y. Wu, Z. Yu, J. Zhang, G. Yang, Q. Yan, J. Li, T. Li, L. Liu, *Front. Cell Dev. Biol.* **2020**, *8*, 214.

[19] I. S. Opstad, 3D SIM data of mitochondria in the cardiomyoblast cell-line H9c2 adapted to either glucose or galactose, **2021**.

SUPPORTING INFORMATION

Additional supporting information may be found in the online version of the article at the publisher's website.